Surface & Coatings Technology 205 (2010) 2134–2141

Contents lists available at ScienceDirect

Surface & Coatings Technology

journal homepage: www.elsevier.com/locate/surfcoat

Structure–property relations in ZrCN coatings for tribological applications

E. Silva [a], M. Rebelo de Figueiredo [b], R. Franz [b], R. Escobar Galindo [c,d], C. Palacio [e], A. Espinosa [e], S. Calderon V. [a,*], C. Mitterer [b], S. Carvalho [a]

[a] Universidade do Minho, Dept. Física, Campus de Azurém, 4800-058 Guimarães, Portugal
[b] Christian Doppler Laboratory for Advanced Hard Coatings, Department of Physical Metallurgy and Materials Testing, University of Leoben, Franz-Josef-Str. 18, 8700 Leoben, Austria
[c] Centro de Micro-análisis de Materiales (CMAM-UAM), Cantoblanco, 28049, Madrid, Spain
[d] Instituto de Ciencia de Materiales de Madrid (ICMM -CSIC), Cantoblanco, 28049, Madrid, Spain
[e] Departamento de Física Aplicada (CXII), Universidad Autónoma de Madrid, Cantoblanco, 28049, Madrid, Spain

ARTICLE INFO

Article history:
Received 1 January 2010
Accepted in revised form 29 August 2010
Available online 7 September 2010

Keywords:
ZrCN
PVD
Magnetron sputtering
Metal-containing coating
Hardness
Tribology

ABSTRACT

ZrCN coatings were deposited by dc reactive magnetron sputtering with N_2 flows ranging from 2 to 10 sccm in order to investigate the influence of the nitrogen incorporation on structure and properties. Information about the chemical composition was obtained by glow discharge optical emission spectroscopy and Rutherford backscattering spectroscopy. The evolution of the crystal structure studied by X-ray diffraction revealed the formation of a face-centred cubic ZrCN phase for N_2 flows greater than 4 sccm. Additionally, the presence of an amorphous phase in the coatings deposited with the highest N_2 flows could be evidenced by Raman spectroscopy and X-ray photoelectron spectroscopy. This phase can act as a lubricant resulting in a low coefficient of friction as shown in the conducted ball-on-disc tests. Nanoindentation measurements showed that coatings deposited with a 6 sccm N_2 flow had the maximum hardness which also revealed the best performance in the conducted dry cutting tests.

1. Introduction

The increasing demand of new materials with enhanced mechanical and tribological properties has strongly encouraged investigations in the field of surface engineering and a wide variety of coatings like diamond-like carbon, transition metal nitrides, carbides and carbonitrides have been developed [1–20]. Among the transition metal nitrides and carbonitrides, Ti-based coatings have been extensively studied and evaluated with respect to industrial applications [8,15]. However, despite the fact that ZrN films have good characteristics concerning hardness, corrosion resistance and tribological performance and, similar to TiCN, significant improvements by carbon addition can be expected, studies concerning the synthesis and properties of ZrCN coatings are quite scarce.

Researchers that investigated ZrCN coatings reported on the synthesis by chemical vapor deposition (CVD) [2,5] and physical vapor deposition (PVD) [2,3,6,7,21] techniques. Rie et al. [5] obtained a ZrCN coating with a dense columnar structure by plasma-assisted CVD. Structural investigations by Larijani et al. [7] showed a variation of the lattice parameter due to the substitution of N atoms by C in the ZrN crystal lattice. Since both compounds, ZrN and ZrC, form a solid solution over the entire composition range, the change of the lattice parameter is in agreement with Vegard's law. Measured hardness values reach up to 1040 HK0.01 [5], 3600 HV0.1 [3], 2500 HV [7] and 28.0 GPa [4] while the highest values are typically observed for a C/N ratio slightly exceeding 1. Investigations by Gu et al. revealed a good corrosion resistance for ZrCN coatings deposited by arc-evaporation which are promising results for the use of these coatings in decorative applications. In terms of cutting behaviour, Kudapa et al. combined TiCN with ZrCN deposited by medium temperature CVD and found an improved abrasion wear resistance and prolonged tool lifetime in machining of nodular iron and 4340 low-alloyed steel [2]. In general, the studies carried out so far indicated that ZrCN coatings could be a promising material in a wide variety of mechanical devices, but studies relating the structure of ZrCN coatings to their properties including mechanical and tribological properties as well as the cutting performance are rare.

In the present work, ZrCN coatings were synthesized by dc reactive magnetron sputtering. The study addresses the influence of the nitrogen concentration on the structure and properties of the coatings, in particular mechanical and tribological properties as well as cutting behaviour. For the latter ZrCN coatings have been deposited onto cermet cutting tools and were compared with a commercial coating serving as a reference for the tests under dry cutting conditions.

2. Experimental part

ZrCN coatings were deposited on (100) single crystalline silicon wafers, high-speed steel (AISI M2) and WC–Co "TNMG 16 04 08-QM H13A" cutting tools for turning by dc reactive magnetron sputtering in an $Ar/N_2/C_2H_2$ atmosphere. The deposition system consists of two

* Corresponding author.
E-mail address: secave44@gmail.com (S. Calderon V.).

0257-8972/$ – see front matter © 2010 Elsevier B.V. All rights reserved.
doi:10.1016/j.surfcoat.2010.08.126

vertically opposed rectangular shaped unbalanced magnetrons of type 2 [22] in a closed field configuration. The current density applied to both Zr targets (200×100×6 mm) was 10 mA/cm^2. Prior to deposition, the substrates were ultrasonically cleaned for 15 min in ethanol, followed by 15 min in acetone and in-situ sputter etched with a constant current of 0.35 A for 15 min in a 0.3 Pa Ar atmosphere.

The base pressure in the chamber was approximately 1×10^{-3} Pa and the total pressure during depositions ranged from 0.33 to 0.46 Pa depending on the gas flows. In order to change the nitrogen content in the coating, the samples were grown with different N_2 flows ranging from 2 to 10 sccm. An Ar flow of 60 sccm and a C_2H_2 flow of 6 sccm were kept constant resulting in a partial pressure of ~0.30 Pa. The substrate bias voltage and the substrate temperature remained constant at −50 V and 200 °C, respectively. A metallic Zr interlayer of ~0.25 μm was deposited in order to improve the adhesion. For comparative purposes, Zr_xN_{1-x} and Zr_xC_{1-x} coatings were deposited with a N_2 flow of 9 sccm and a C_2H_2 flow of 10 sccm, respectively, while all other deposition parameters remained unaltered.

In order to analyze the chemical composition of the coatings, glow discharge optical emission spectroscopy (GDOES) and Rutherford backscattering spectroscopy (RBS) were carried out. GDOES experiments were performed using a Jobin Yvon RF GD Profiler equipped with a 4 mm diameter anode and operating at a typical radio frequency discharge pressure of 650 Pa and a power of 40 W. The setup was calibrated using standard materials of known composition. In order to improve the quantification of nitrogen, a series of nitride coatings deposited by magnetron sputtering was used as calibration samples [23]. RBS experiments were performed with a 5 MV HVEE Tandetron [24], and the spectra were collected using 2 MeV H^+ ions at an ion dose of 7 μC. The data were acquired simultaneously with two silicon surface barrier detectors located at scattering angles of 170° and 135°, respectively, and with an energy resolution of 16 keV. The experimental spectra were fitted with the software program RBX [25].

Fracture cross-sections of the synthesised coatings were examined on a conventional Scanning Electron Microscope (SEM) model LEICA S360. The sample thickness was derived from an average number of three 'ball-cratering' experiments on each sample. The structure and phase composition of the coatings were assessed by X-ray diffraction (XRD) using a conventional Philips PW 1710 diffractometer with Cu Kα radiation operating in the Bragg–Brentano configuration.

Raman spectra were acquired with a Jobin-Yvon HR 460 monochromator and a nitrogen cooled CCD. The excitation light was the 514.5 nm line of an Ar–Kr laser. The incident and scattered beams were focused using an Olympus microscope and a Kaiser Super-Notch filter was used to suppress the elastic scattered light. X-ray photoelectron spectroscopy (XPS) measurements were performed using a hemispherical analyzer and Mg Kα radiation from an X-ray source operated at 300 W constant power. The pass energy was 9 eV giving a constant resolution of 0.9 eV [26]. In order to minimize surface contamination problems, a moderate energy sputter cleaning process was performed with Ar^+ for 10 min before analysis.

Hardness measurements according to Oliver and Pharr [27,28] were conducted using a MicroMaterials Nanotest system equipped with a Berkovich indenter applying a maximum load of 15 mN. The tribological tests were performed on a ball-on-disc tribometer from CSM Instruments using alumina balls as counterparts (purity of 99.8% and Ø 6 mm). The tests were conducted at room temperature applying a normal load of 1 N, a sliding speed of 0.1 m/s as well as a constant wear track radius of 7 mm and a sliding distance of 220 m (5000 laps). No lubricant was applied. Subsequent to the tribological tests, the worn-off volume of the coatings was evaluated by an optical 3D white light profiling system (Wyko NT 1000) at 5 areas evenly distributed on the circumference of the wear track. From these measurements, the removed volume was determined and the wear coefficient calculated as the ratio between volume and applied load times sliding distance [29].

A Cincinnati Milacron Hawk-150 numerically controlled lathe was used to perform turning tests, which were performed with a cutting speed of 200 m/s, a feed rate of 0.1 mm/rot and 1 mm depth of cut. The working material chosen was a usual commercial alloy steel, (0.30% C; 0.40% Si; 0.45% Mn; 2.00% Cr; 0.40% Mo; and 2.00% Ni) with main applications in shafts, bearings and some plastic moulds. Dry turning was used, though eliminating coolant increases the amount of heat at the cutting zone, creating the potential for premature tool wear. The following conventional tool wear parameters were measured by SEM: VB — flank wear, VB_{MAX} — maximum flank wear, KM — distance between tool edge and crater centre (rake face). After the turning tests, the dominant wear mechanisms were revealed by morphological and chemical modifications observed by SEM coupled with an energy-dispersive X-ray spectrometry (EDS) microanalyzer. The commercial cutting tool (one of the best solutions actually available in the market for high-speed turning) used as a reference in the cutting tests was synthesized by CVD. The coating had a multilayer architecture comprising a 8.8 μm Ti(C,N) base layer, a 4.3 μm intermediate Al_2O_3 layer and a 1.6 μm top TiN layer.

3. Results and discussion

3.1. Deposition rate and chemical composition

The deposition rate of the ZrCN coatings decreases from 2.1 to 1.1 μm/h with increasing N_2 flow. This behaviour can be explained by a progressive poisoning of the targets since the target potential increases from −335 to −390 V. In the case of the Zr_xN_{1-x} coating, the even lower deposition rate of 0.7 μm/h is associated to a target potential of ~−400 V. For the Zr_xC_{1-x} coating an inverse behaviour was observed with a higher deposition rate of 1.8 μm/h and a lower potential of ~−280 V.

Table 1 shows the chemical composition of the coatings obtained from average values measured by GDOES and RBS. As expected, the nitrogen content increases from 9 to 48 at.% with increasing N_2 flow during deposition. This evolution is accompanied by a strong decrease of the Zr content from 78 to 35 at.%. The decrease of the Zr content and the increase of the N content are, in the first place, due to the change of the gas composition. Secondly the progressive poisoning of the targets at higher N_2 gas flows probably further enhances the reduction

Table 1
Deposition parameters, chemical composition and mechanical and tribological properties.

Zr C+N (Regime)	Sample	N2 gas flow (sccm)	Thickness (μm)	Dep. rate (μm h^{-1})	Chemical composition % at.				H (GPa)	E (GPa)	COF	Wear rate (m3N-1 Lap-1×10^{-15})
					Zr	N	C	O				
–	$ZrxC_{1-x}$	–	3.5	1.8	59	2	35	4	12.0±1.6	210.0±14.3	–	–
–	$ZrxN_{1-x}$	9	1.5	0.7	47	44	2	7	20.0±1.5	260.2±22.3	–	–
≥2.9 (Regime I)	1	2	6.9	2.1	78	9	8	5	13.1±0.9	185.8±11.1	0.5	–
	2	4	5.8	2.1	70	16	8	6	15.1±0.8	181.9±8.2	0.5	–
=1.3 (Regime II)	3	6	5.3	1.7	54	31	10	5	29.2±3.2	294.9±32.1	0.6	2.27±0.25
≤0.7 (Regime III)	4	8	3.1	1.5	40	44	10	6	18.0±3.4	234.7±41.1	0.2	1.79±0.57
	5	10	3.0	1.1	35	48	12	5	17.1±2.5	242.0±20.7	0.1	0.38±0.97

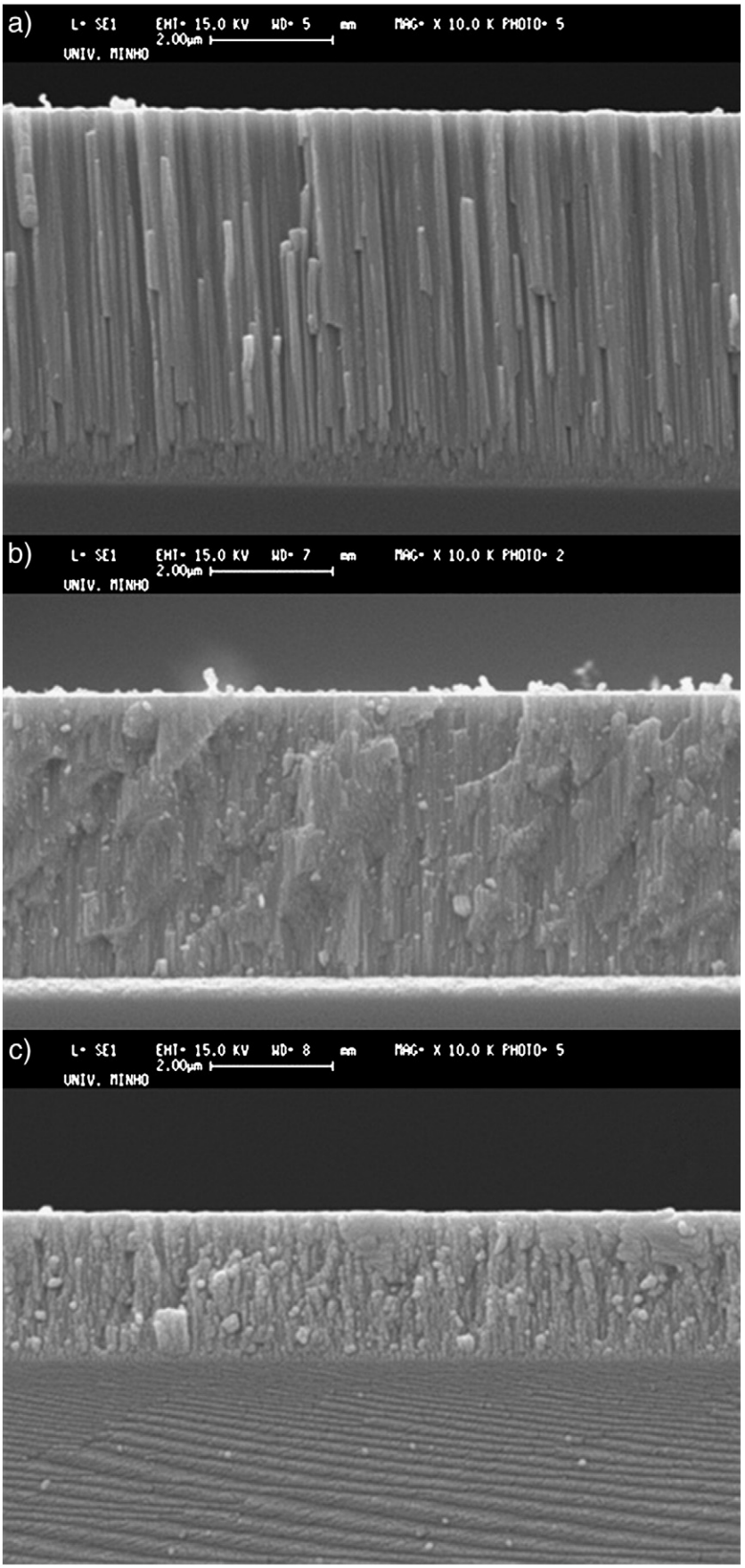

Fig. 1. SEM fracture cross-sections of coatings synthesized at different N_2 flows: a) 2 sccm, b) 6 sccm and c) 10 sccm.

of Zr. Furthermore, the carbon content increases only slightly from 8 to 12 at.%, whereas the oxygen content resulting from the high base pressure and consequently residual atmosphere in the chamber remains almost constant at 5 to 7 at.%. The highest oxygen incorporation could also be due to the low deposition rate. Particularly Oliveira et al. [30] reported the unavoidable incorporation of oxygen by the residual oxygen present in the deposition chamber, due to the low deposition rate. From a detailed analysis of the chemical composition shown in Table 1, three different compositional regimes for the ZrCN samples can be derived as a function of the Zr/(N + C) atomic ratio. Regime I corresponds to an atomic ratio of Zr/(C + N) ≥ 2.9, Regime II to Zr/(C + N) = 1.3 and Regime III to Zr/(C + N) ≤ 0.7. This classification into three different regimes will facilitate the discussion of the results in the following sections.

3.2. Structure

The morphology of the coatings is disclosed by the cross-sectional SEM micrographs of fractured samples as shown in Fig. 1. The coatings of Regime I (see Fig. 1a)) present a columnar morphology, typical for coatings grown under low energetic ion bombardment, limited adatom mobility conditions and high deposition rate [31]. These coatings are also porous with voids between fiber-shaped columns and resemble those films of Zone I of the Thornton's structure zone model where the voided growth defects are a consequence of atomic shadowing and limited surface diffusion [32]. Continuing with Regime II (see Fig. 1b)), the appearance of the coatings changes to a very fine-grained, dense morphology. This evolution can be explained by the decrease of the deposition rate which is a result of more pronounced target poisoning as discussed above and the increasing nitrogen content, which gives rise to a growth transition from columnar metallic to fine-grained carbonitrides. In Regime III a fine-globular morphology is visible (see Fig. 1c)) caused by the excess carbon and nitrogen (see Table 1) resulting in continuous renucleation of grains. The main feature of this structure type is the presence of small grains since grain growth by coalescence is strongly restricted due to limited mobility of grain boundaries covered with excess nitrogen and/or carbon [33,34].

The X-ray diffraction patterns of all synthesized ZrCN coatings are displayed in Fig. 2 as well as the patterns of Zr_xC_{1-x} and Zr_xN_{1-x} for comparison.

According the phase diagram presented on Fig. 3 reported by Binder et al. [35], Zr can incorporate high fractions of N and form an α-Zr phase. This situation is different for C where only small fractions can be incorporated. Taking into account the Zr contents of 78 and

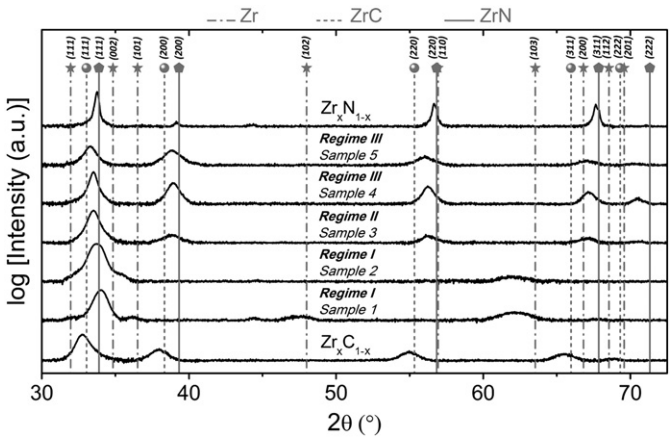

Fig. 2. XRD diffractograms of Zr_xN_{1-x}, Zr–C–N for the different Regimes and Zr_xC_{1-x}. Peak positions obtained from the database of the International Centre for Diffraction Data (ICDD) for the materials ZrN (ICDD card no. 035-0753), ZrC (ICDD card no. 035-0784) and Zr (ICDD card no. 1-1147) are indicated as a reference.

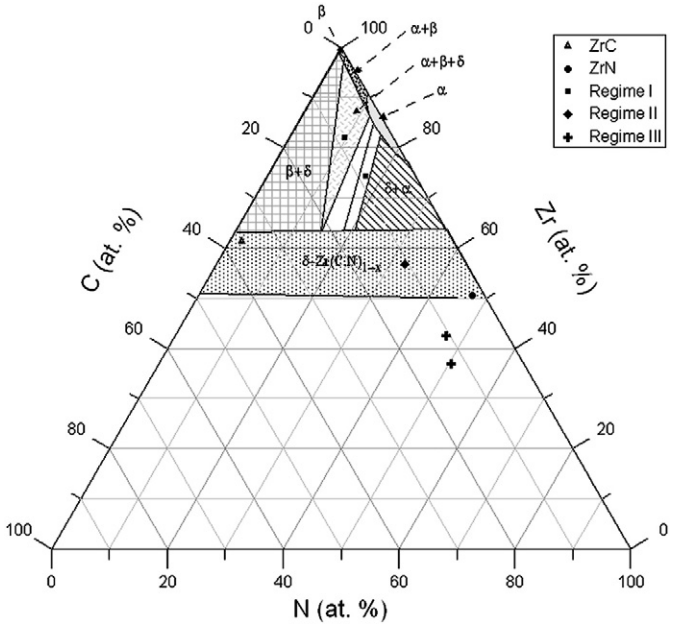

Fig. 3. Plot of the chemical composition of all prepared samples in the ZrCN phase diagram according to [28].

70 at.% and the N content of 9 and 16 at.% for the coatings in Regime I ((Zr/(C + N) ≥ 2.9), it seems reasonable that mainly a metallic α-Zr phase is formed. It is not clear how the C and the O are incorporated. They probably form phases that are not detectable by XRD.

In Regime II (Zr/(C + N) = 1.3) a face-centred cubic (fcc) ZrN type structure is visible, with a (111) preferred orientation. The peak broadening and the shift to lower angles compared to the Zr_xN_{1-x} pattern for this coating can be explained by the higher fraction of C atoms in N positions on the ZrN structure inducing the formation of a ZrCN solid solution [36]. In Regime III (Zr/(C + N) ≤ 0.7) the coatings retain the fcc crystal structure, but present a lower degree of crystallinity and the preferred orientation changes. However, the low Zr/(C + N) ratio suggests the presence of an additional, X-ray amorphous phase, most likely amorphous excess C or CN_x. Indeed, these phases were also observed within the TiCN system [37]. The formation of this phase can hinder continuous grain growth and stimulate permanent renucleation as described by Barna [38], which is in agreement with the morphology evolution of these coatings previously discussed.

In order to better understand the structural evolution, coatings from the three different regimes were analyzed by Raman spectroscopy as shown in Fig. 4. For the Regime I coatings, the spectra show a large number of very weak and broad bands centred at around 151 and 203 cm^{-1} for acoustic modes, and at 480 and 560 cm^{-1} for ZrN optic modes, slightly shifted as compared to literature values [39,40]. These forbidden bands are activated by the presence of crystalline defects expected by the growth process, as discussed before in the XRD results [41,42]. For the Regime II coating the same bands are visible, but there is an increase in intensity in the first order bands, which may be explained by the decrease of the Zr/(N + C) atomic ratio and an increase of the fcc ZrN phase. In the region between 1250 and 1595 cm^{-1} several authors assigned carbon phases like C—N at 1250 cm^{-1} and C=N at 1500 cm^{-1}[43] as well as D and G bands of carbon materials at 1370 and 1580 cm^{-1} [44]. The similarity of the vibrational frequencies of C–C and C–N and consequently the broad band modes make the interpretation of the results difficult. For the coatings of Regime III, the same features as for Regime II are found. The vibration frequencies of solid carbon nitrides are expected to be close to the modes of the analogous unsaturated CN_x molecules, which are 1500–1600 cm^{-1} for chain-like molecules and 1300–

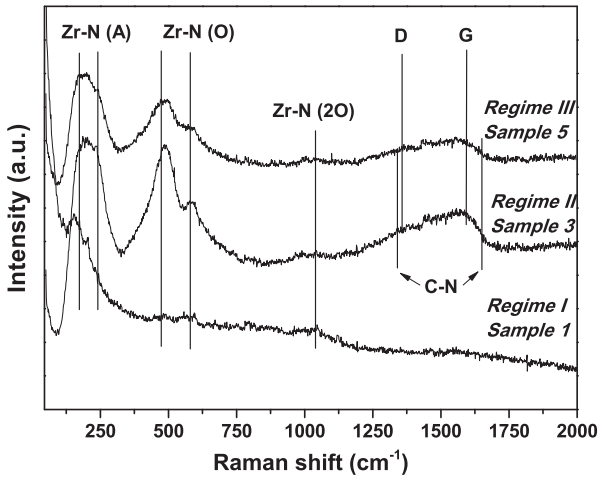

Fig. 4. Raman spectra of the Zr–C–N coatings grown for the different Regimes.

1600 cm^{-1} for ring-like molecules [43]. This means that there is no distinction in the D and G band region between modes due to C or to N atoms sp^2 hybridized bonding, probably due to the dominating structure of the amorphous CN_x material. The low Zr/(N + C) ratio suggests, besides a ZrCN crystalline phase, the formation of an additional a-CN_x amorphous phase.

A thorough analysis by XPS was conducted to gain additional information about the chemical bonding state of the coatings. The Zr 3d core level spectra are characterized by the doublet terms Zr $3d_{3/2}$ and Zr $3d_{5/2}$ due to spin-orbit coupling. Upon fixing the intensity ratio of the peaks at 1.6 and the spin-orbit splitting at 2.4 eV, it was possible to perform a deconvolution of the Zr 3d spectra in terms of the different chemical states: nitride (180.0 eV), carbide (179.5 eV), oxynitride (181.9 eV) and oxide (182.9 eV), in agreement with literature values [44]. For simplicity, the following discussion will only refer to the position of the Zr $3d_{5/2}$ term, assuming that the Zr $3d_{3/2}$ is placed at 2.4 eV higher binding energies.

Fig. 5 shows the N(1s), C(1s) and Zr(3d) core level spectra of coatings from Regime I (Zr/(N + C) ≥ 2.9) and Regime III (Zr/(N + C) ≤ 0.7). The spectra of Zr_xC_{1-x} and Zr_xN_{1-x} are also illustrated for comparison.

In the Zr 3d spectrum of the Zr_xN_{1-x} sample, the main component is ascribed to Zr–N bonds (180.0 eV). The other two contributions, located at 181.9 and 182.9 eV correspond to Zr–O–N and Zr–O bonds, respectively [45]. In the C 1s spectrum it is possible to detect a small contribution centred at 285.5 eV that can be attributed to C–N sp2 bonding. The main component (397.0 eV) of the N 1s spectrum is related to N–Zr bonds in agreement with literature values [46]. For Zr_xN_{1-x} one more small contribution is observed at 399.4 eV, assigned by several authors to N–C sp2. These bonds are located in the region between 399.9 eV [47] and 400.6 eV [26]. The presence of this signal is in accordance with the C 1s spectrum where these C–N bonds are also detected.

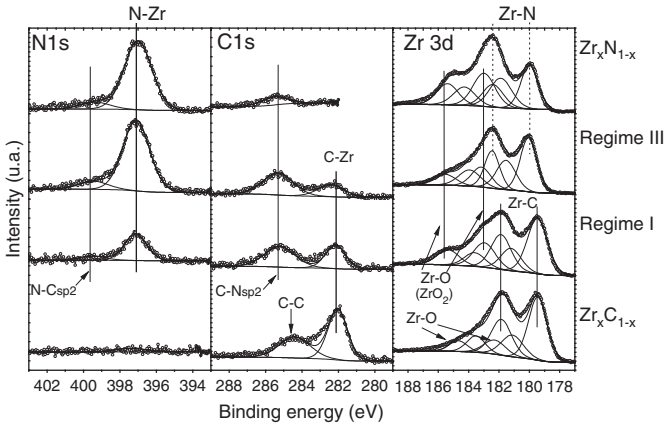

Fig. 5. X-ray photoelectron spectrum of N(1s), C(1s) and Zr(3d) electrons of Zr_xN_{1-x}, ZrCN and Zr_xC_{1-x} coatings.

The Zr 3d spectrum of Zr_xC_{1-x} shows a main component ascribed to Zr–C bonds (179.5 eV). The analysis of the second main component of the sample is more complex. The component is centred at approximately 181.1 eV. This sample has a lower N/O than C/O ratio and therefore this component was assigned to Zr–C–O bonds. Although no references could be found in the literature, it is plausible that such a phase is present considering the measured oxygen content. The last contribution found at energies higher than 182.0 eV is attributed to zirconium oxide formation [45,46]. In the C 1s spectra it is possible to see for the Zr_xC_{1-x} sample the main component centred at 282.2 eV, corresponding to the C–Zr bonds of zirconium carbides and the second contribution at 284.4 eV can be associated to the C–C bonds of graphite. Concerning the ZrCN coating in Regime I, the Zr 3d spectrum shows three different components. At a binding energy of 182.9 eV there is a contribution usually related in literature to the formation of ZrO_2. For lower binding energies (181.2 eV) there is a second significant contribution assigned to Zr–C–O bonds as discussed before for the Zr_xC_{1-x} sample. However, the main component is ascribed to Zr–C bonds at 179.5 eV. This Zr–C bonding is confirmed in the C 1s spectrum where the peak at lower energies (282.2 eV) is related in the literature to C–Zr bonds [45]. A second contribution is centred at 285.1 eV and can be associated to C–N sp2 bonds. [26,43] The main component of the N 1s spectrum, centred at 397.1 eV, is ascribed to N–Zr bonds [46]. A small contribution for N–C sp2 bonds can be observed centred at 399.3 eV in concordance with the C–N sp2 bonds observed in the C 1s spectrum.

For the last regime analyzed (i.e., Regime III with Zr/(N + C) ≤ 0.7), the Zr 3d spectrum shows the main component ascribed to Zr–N bonds (180.1 eV) [46]. The second component is centred at 181.5 eV, between 181.1 eV (related to Zr–C–O formation) and 181.9 eV (Zr–O–N). This sample has similar N/O and C/O atomic ratios, therefore,

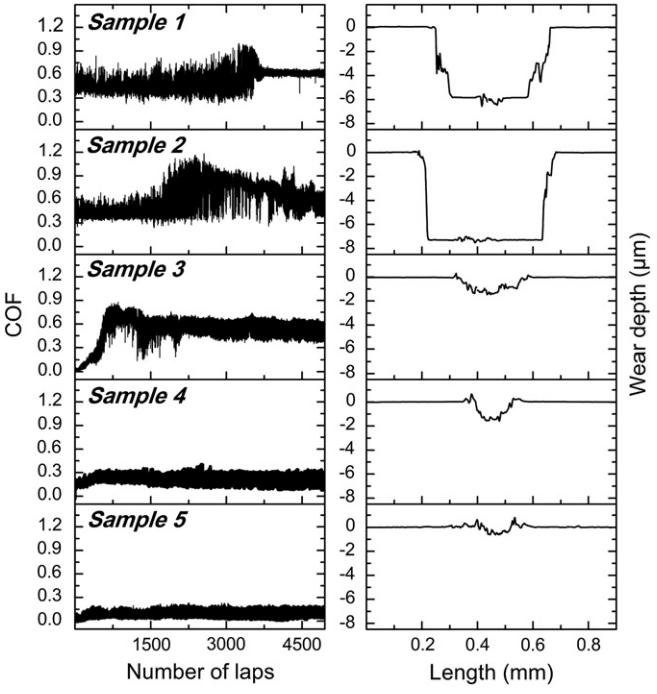

Fig. 6. Frictions curves and wear depths from the tribological tests of ZrCN coatings.

Table 2
Cutting behaviour of turning tools with coatings grown with different N2 flow and commercial tool for comparison purposes.

Tool/Coat. (N_2 flow)	Volume removed [cm^3]	Cutting time [min]	Wear type	Obs.
Commercial	310.5	15.5	VB ≈ 90 μm VB_{MAX} ≈ 60 μm KM ≈ 180 μm	Continues chip
2	46.8	2.3	Catastrophic failure	Tool tip broken
4	171.1	8.6	Catastrophic failure	Tool tip broken
6	310.5	15.5	VB ≈ 110 μm VB_{MAX} ≈ 190 μm KM ≈ 120 μm	Fragmented chip
8	72.0	3.6	Catastrophic failure	Tool tip broken
10	45.11	2.3	Catastrophic failure	Tool tip broken

suggesting that both Zr–C–O and Zr–O–N bonds are present. Finally, the component centred at 183.2 eV is ascribed to ZrO_2 [45]. In the C 1s spectrum, the C–Zr component is centred at 282.4 eV, that is shifted by 0.2 eV towards higher energies in comparison to the carbide peak of Regime I. This denotes the presence of a higher oxidation state for this compound, in agreement with the Zr 3d results of this sample discussed above [26,45,46]. The main component is observed at 285.3 eV and can be associated to C–N sp2 bonds, confirmed by N 1s spectra where the presence of N–C sp2 bonds (399.5 eV) is clearly visible. These results explain the presence of a a-CN_x phase, supported by the low Zr/(N + C) ratio. Finally, the main component in this spectrum (397.1 eV) again corresponds to N–Zr bonds.

It should be pointed out that a small fraction of O and C can be partially incorporated on the ZrCN solid solution.

3.3. Mechanical and tribological properties

Hardness and Young's modulus of the ZrCN coatings are shown in Table 1. The structural changes are consistent with the evolution of these mechanical properties. As shown in Table 1, the coatings of Regime I show a low hardness due to the high zirconium content. The small increase of nitrogen incorporated results in a slight increase in hardness from 13.1 ± 0.9 to 15.1 ± 0.8 GPa which can be explained by the decrease on the Zr content. For the coating in Regime II, both the chemical composition and structure suggest the formation of a ZrCN solid solution. The hardness obtained for this Regime (H = 29.2 ± 3.2 GPa) is in agreement with values reported by other authors H (ZrCN) = 25.4 − 48.5 GPa [6,7,20]. Finally, for the coatings in Regime III the drastic reduction of hardness can be associated to the presence of soft amorphous phases like a-CN_x with H(a-CN_x) = 9.5 − 16 GPa [44] and a-C with H(a-C) = 15 − 20 GPa [12]) as discussed before.

Regarding coating stiffness and according to Carvalho et al. [31], the columnar structure visible in SEM fracture cross-sections for Regime I coatings may justify the low Young's modulus values measured (E < 190 GPa). The highest value is observed for the Regime II coating (E = 294.9 ± 32.1 GPa) which presents a compact and fine-grained morphology. For the coatings in Regime III, the observed reduction on the Young's modulus (E < 245 GPa) should be related with the development of some amorphous phases.

Finally, differences between the three defined regimes can also be observed for the tribological properties as shown in Fig. 6. The coatings from Regime I, with its columnar and porous microstructure, reveal a rather high coefficient of friction (COF) of ~0.5 and an early failure in the performed ball-on-disc tests. For the coating in Regime II, a slight increase of the COF to ~0.6 and a pronounced running-in period can be noticed, but this coating is not worn through during the test. Obviously the change in the microstructure is beneficial for the wear resistance of ZrCN and the obtained values for friction and wear are consistent with results found in the literature [1,20,48]. In contrast to the other coatings, the ZrCN coatings in Regime III show a low friction with the COF in the range of 0.1–0.2 and a moderate wear. This low-friction behaviour is a result of the presence of an amorphous CN_x phase which is known to be a lubricant phase and, hence, significantly reduces the friction as was already well reported on [49,50].

3.4. Cutting performance

From the performed dry cutting tests, an evident trend is the low cutting time of the majority of the coatings as shown in Table 2. The coatings grown on Regime I and III presented a catastrophic failure with fracture of the cutting edge after a cutting time between 2.3 and 8.6 min. This type of failure appears when the cutting speed is too high [51]. The tool with the ZrCN coating of Regime II presented wear parameters similar to the commercial tool tested. After a cutting time of 15.5 min this tool presented a flank wear of 110 μm and a maximum flank wear of 190 μm compared to 90 μm and 160 μm, respectively, of the commercial tool.

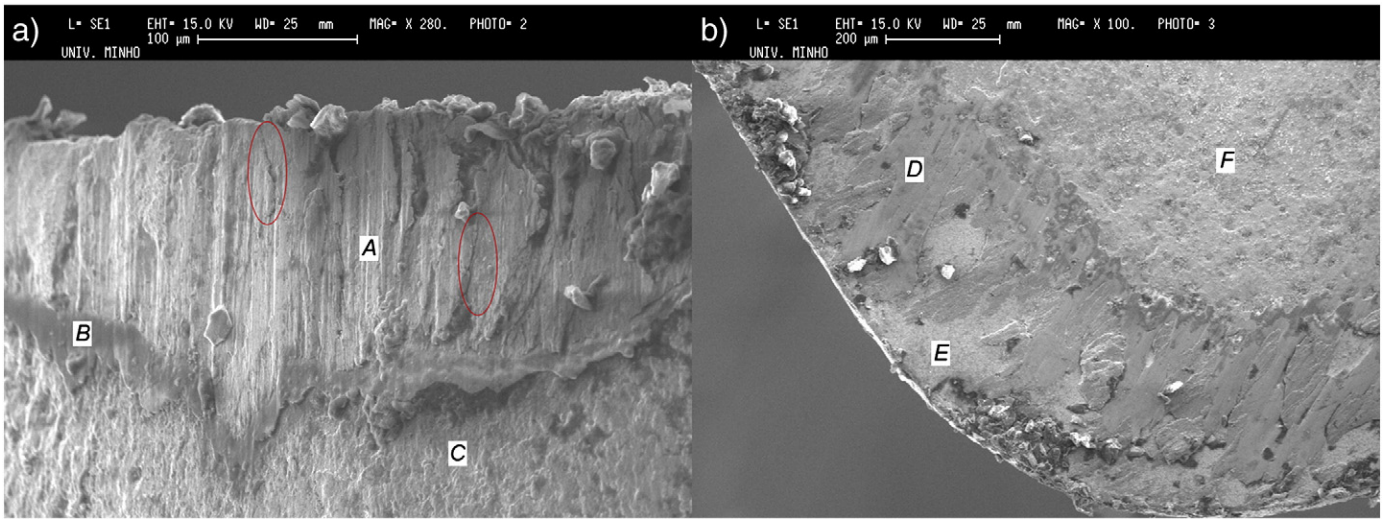

Fig. 7. SEM image of the cutting edge of the tool deposited with the ZrCN coating from Regime II showing a) flank face wear and b) rake face wear. The squares assigned with letters correspond to EDS analyzed areas and the balloons indicate micro fractures in the tool.

Table 3
Chemical elements present in the analyzed areas.

Zone	Chemical elements		
A	Fe	O	Fe
B	Si	Mn	O
C	Fe	Zr	O
D	Zr	O	–
E	W	Fe	O
F	Zr	Fe	O

Another remarkable result is the chip form obtained by testing the ZrCN coating of Regime II. For this tool, the formed chips were fragmented in small pieces instead of continuous chips resulting from the operation with the commercial tool. The difference of the chip form can be explained by the smaller KM of ZrCN of Regime II as compared to commercial tool [51]. In terms of production processes, such a fragmented chip form is very beneficial because it can be removed more easily and is less dangerous for operators. In addition, they can also result in an improved surface quality of the workpieces and the easier heat dissipation helps to increase the tool lifetime.

In order to obtain more information about wear mechanisms present on the tool coated with the Regime II ZrCN, the tool tip was analyzed by SEM and EDS. In Fig. 7a) grooves in the flank face that are perpendicular to the cutting edge can be observed indicating abrasive wear as already discussed in the literature [51–53]. Additionally, thermal fractures with increasing concentration towards the tool tip are visible as well. These two different types of wear are also confirmed by the analysis of the rake face (Fig. 7b) where the same features can be observed.

The above described wear mechanisms are confirmed by chemical analyses using EDS. In Table 3 the chemical elements present in each signed area on the tool tip as shown in Fig. 7 are summarized. Due to oxidation, during the cutting operation, oxides originating from the coating (Zr–O), the tool (W–O) and the workpiece (Fe–O) were detected. Oxidation occurs since the temperature at the cutting edge can reach values up to 1000 °C [54] during operation. The typically detected iron contamination originated from the workpiece while the adherence of the workpiece material can be attributed to both, the high plasticity of the austenitic fcc structure that hardens rapidly and its reactivity with the tool material [55,56]. These mechanisms are associated to the high temperatures reached during the cutting tests inducing the above described thermal cracks [57].

The promising cutting performance of the ZrCN coating from Regime II can be correlated to the mechanical properties. As shown in Fig. 8, the best cutting performance was observed for the coating with the highest hardness and Young's modulus. These points towards an improvement of the strength of the coated tool due to the superior mechanical properties of the Regime II coating. As discussed above, the enhancement of the mechanical properties of this coating results from the formation of a ZrCN solid solution. On the other hand, the formation of a lubricious CN_x phase which significantly reduced the friction of the coatings in Regime III apparently does not improve the in-service behaviour.

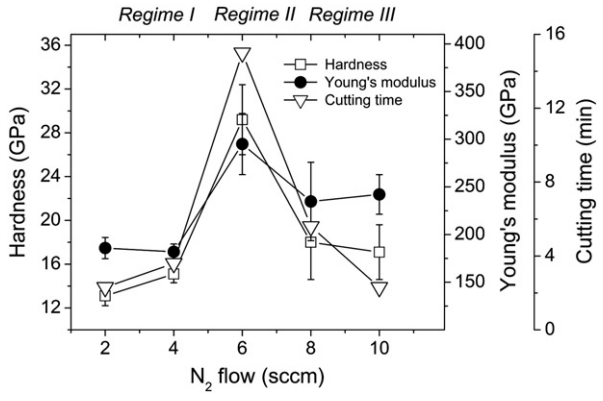

Fig. 8. Hardness, Young's modulus and cutting time in a function of N_2 flow.

4. Conclusions

In the present study, ZrCN coatings were successfully synthesized by magnetron sputtering as a function of N_2 flow and the observed structure could be related to their mechanical and tribological properties. By the compositional analysis the nitrogen content increases from 9 to 48 at.% with increasing N_2 flow during deposition. This evolution is accompanied by a strong decrease of the Zr content from 78 to 35 at.%. Additionally the carbon content increases only slightly from 8 to 12 at.%.

Low nitrogen fractions in the coating result in less dense columnar coatings with a low hardness and a low wear resistance. The optimum in a hardness of ~29 GPa was found for the coating with $Zr/(C+N) = 1.3$. This coating presents a dense microstructure and the increase in hardness can be associated to the formation of a ZrCN solid solution. Tribological tests with this coating revealed a high friction, but moderate wear. A drop of the coefficient of friction to 0.1–0.2 could be observed for the coatings with $Zr/(C+N) \leq 0.7$, which is related to the formation of an additional amorphous CN_x phase. However, these coatings show a lower hardness (17–18 GPa), but moderate wear in the ball-on-disc tests. The best performance in dry cutting tests was obtained for the coating with $Zr/(C+N) = 1.3$ which is comparable to the results of a commercial coating serving as a reference. Apparently the higher hardness and Young's modulus beneficially influenced the cutting behaviour, whereas an improvement due to the formation of a low-friction phase could not be noticed. In summary, the observed properties of ZrCN and their relation to crystal structure and chemical bonding offer a good basis for the development of coatings for tribological applications.

Acknowledgments

The authors are grateful to Dr. Alicia Andrés, Instituto de Ciencia de Materiales de Madrid (ICMM-CSIC), for her assistance in carrying out the Raman spectroscopic analysis, as well as the financial support of the CRUP Institution by the project "Acção No. E — 1007/08" and PTDC/CTM/102853/2008. This work was also financially supported by the Spanish Ministry of Science and Innovation (Projects FUNCOAT CSD2008-00023 and HP2007-0116). Financial support by the Christian Doppler Research Association within the framework of the CD lab 'Advanced Hard Coatings' with its partners PLANSEE Composite Materials(Lechbruck, Germany) and OC Oerlikon Balzers AG (Balzers, Liechtenstein) is highly acknowledged as well.

References

[1] S.H. Yao, Y.L. Su, W.H. Kao, K.W. Cheng, Mater. Lett. 3230 (2005) 59.
[2] S. Kudapa, K. Narasimhan, P. Boppana, W.C. Russel, Surf. Coat. Technol. 120–121 (1999) 259.
[3] E. Grigore, C. Ruset, X. Li, H. Dong, Surf. Coat. Technol. 204 (2010) 1889.
[4] M. Balaceanu, T. Petreus, V. Braic, C.N. Zoita, A. Vladescu, C.E. Cotrutz, M. Braic, Surf. Coat. Technol. 204 (2010) 2046.
[5] K.-T. Rie, J. Wöhle, Surf. Coat. Technol. 112 (1999) 226.
[6] Gu. Jian-De, Pei-Li Chen, Surf. Coat. Technol. 200 (2006) 3341.
[7] M.M. Larijani, M.B. Zanjanbar, A. Majdabadi, J. Alloys Compd. 492 (2010) 735.
[8] S. Vepřek, P. Nesládek, A. Niederhofer, F. Glatz, M. Jílek, M. Šíma, Surf. Coat. Technol. 108–109 (1998) 138.
[9] J. Musil, H. Poláková, Surf. Coat. Technol. 99 (2000) 127.
[10] S. Carvalho, E. Ribeiro, L. Rebouta, C. Tavares, J.P. Mendonça, A. Caetano Monteiro, N.J.M. Carvalho, J.Th.M. De Hosson, A. Cavaleiro, Surf. Coat. Technol. 459 (2004) 177.
[11] S.K. Field, M. Jarratt, D.G. Teer, Tribol. Int. 949 (2004) 37.
[12] T. Zehnder, J. Patscheider, Surf. Coat. Technol. 138 (2000) 133.

[13] J. Soldán, J. Neidhardt, B. Sartory, R. Kaindl, R. Čerstvý, P.H. Mayrhofer, R. Tessadri, P. Polcik, M. Lechthaler, C. Mitterer, Surf. Coat. Technol. 3555 (2008) 202.
[14] D. Martínez-Martínez, J.C. Sánchez-López, T.C. Rojas, A. Fernández, P. Eaton, M. Belin, Thin Solid Films 64 (2005) 472.
[15] L. Karlsson, L. Hultman, M.P. Johansson, J.E. Sundgren, H. Ljungcrantz, Surf. Coat. Technol. 126 (2000) 1.
[16] S.J. Bull, D.G. Bhat, M.H. Staia, Surf. Coat. Technol. 499 (2003) 163.
[17] S.J. Bull, D.G. Bhat, M.H. Staia, Surf. Coat. Technol. 507 (2003) 163.
[18] T. Polcar, R. Novák, P. Široký, Wear 40 (2006) 260.
[19] M. Rebelo de Figueiredo, J. Neidhardt, R. Kaindl, A. Reiter, R. Tessadri, C. Mitterer, Wear 525 (2008) 265.
[20] M. Balaceanu, M. Braic, V. Braic, G. Pavelescu, Surf. Coat. Technol. 1084 (2005) 200.
[21] I.A. Khan, S. Jabbar, T. Hussain, M. Hassan, R. Ahmad, M. Zakaullah, R.S. Rawat, Nucl. Instrum. Meth. Phys. Res. B 268 (2010) 2228.
[22] B. Window, N. Savvides, J. Vac. Sci. Technol. A 4 (1986) 96.
[23] R. Escobar Galindo, E. Forniés, R. Gago, J.M. Albella, J. Anal. At. Spectrom. 1512 (2007) 22.
[24] A. Climent-Font, F. Pászti, G. García, M.T. Fernández-Jiménez y, F. Agulló, Nucl. Instrum. Methods Phys. Res. B 219 (2004) 400.
[25] E. Kotai, Nucl. Instrum. Methods Phys. Res. B 85 (1994) 588.
[26] C. Palacio, A. Arranz, Surf. Sci. 600 (2006) 2385.
[27] D.P. Dowling, P.V. Kola, K. Donnelly, T.C. Kelly, K. Brumitt, L. Lloyd, R. Eloy, M. Therin, N. Weill, Diamond Relat. Mater. 390 (1997) 6.
[28] J.M. Antunes, A. Cavaleiro, L.F. Menezes, M.I. Simões, J.V. Fernandes, Surf. Coat. Technol. 27 (2002) 149.
[29] E. Rabinowicz, Friction and Wear of Materials, John Wiley, New York, 1964.
[30] A. Oliveira, A. Cavaleiro, M.T. Vieira, Surf. Coat. Technol. 60 (1993) 463.
[31] S. Carvalho, E. Ribeiro, L. Rebouta, F. Vaz, E. Alves, D. Schneider, A. Cavaleiro, Surf. Coat. Technol. 174–175 (2003) 984.
[32] J.A. Thornton, Annu. Rev. Mater. Sci. 293 (1977) 7.
[33] M.A. Adamik, P.B. Barna, I. Tomov, Thin Solid Films 64 (1998) 317.
[34] J. Musil, J. Vlček, Surf. Coat. Technol. 557 (2001) 142.
[35] S. Binder, W. Lengauer, P. Ettmayer, J. Bauer, J. Debuigne, M. Bohn, J. Alloys Compd. 217 (1995) 128.
[36] Cheng-Shi Chen, Chuan-Pu Liu, J. Non-Cryst. Solids 3725 (2005) 351.
[37] D. Martinéz-Martínez, C. López-Cartes, A. Just, A. Fernández, J.C. Sánchez-López, Solid State Sci. 11 (2009) 660.
[38] P.B. Barna, M. Adamik, Thin Solid Films 317 (1998) 27.
[39] C.P. Constable, J. Yarwood, W.-D. Münz, Surf. Coat. Technol. 116–119 (1999) 155.
[40] W. Spengler, R. Kaiser, Solid State Commun. 18 (1976) 881.
[41] A.C. Fernandes, L. Cunha, C. Moura, F. Vaz, P. Carvalho, E. Le Bourhis, Ph. Goudeau, J.P. Rivière, N.M.G. Parreira, Surf. Coat. Technol. 202 (2007) 946.
[42] C. Moura, P. Carvalho, F. Vaz, L. Cunha, E. Alves, Thin Solid Films 515 (2006) 1132.
[43] A.K.M.S. Chowdhury, D.C. Cameron, M.S.J. Hashmi, Surf. Coat. Technol. 112 (1999) 133.
[44] R. Kurt, R. Sanjines, A. Karimi, F. Lévy, Diamond Relat. Mater. 566 (2000) 9.
[45] M. Matsuoka, S. Isotani, W. Sucasaire, N. Kuratani, K. Ogata, Surf. Coat. Technol. 202 (2008) 3129.
[46] P. Carvalho, J.M. Chappé, L. Cunha, S. Lanceros-Méndez, P. Alpuim, F. Vaz, E. Alves, C. Rousselot, J.P. Espinós, A.R. González-Elipe, J. Appl. Phys. 103 (2008) 104907.
[47] Y. Gao, J. Wei, D.H. Zhang, Z.Q. Mo, P. Hing, X. Shi, Thin Solid Films 377–378 (2000) 562.
[48] M. Balaceanu, V. Braic, A. Kiss, C.N. Zoita, A. Vladescu, M. Braic, I. Tudor, A. Popescu, R. Ripeanu, C. Logofatu, C.C. Negrila, Surf. Coat. Technol. 202 (2008) 3981.
[49] J.C. Sánchez-López, D. Martínez-Martínez, C. López-Cartes, Fernández A., Surf. Coat. Technol. 4011 (2008) 202.
[50] C. Quirós, R. Núñez, P. Prieto, E. Elizalde, A. Fernández, C. Schubert, C. Donnet, J.M. Sanz, Vacuum 199 (1999) 52.
[51] "El Mecanizado Moderno — Manual practico", ed. Sandvik Coromant, Sandviken, 1994, Sweden.
[52] R.P. Martinho, F.J.G. Silva, A.P.M. Baptista, Wear 263 (2007) 1417.
[53] Anselmo Eduardo Diniz, Adilson José de Oliveira, J. Mater. Process. Technol. 195 (2008) 275.
[54] E. Ceretti, L. Filice, D. Umbrello, F. Micari, Annals of the CIRP Vol. 56/1/200.
[55] A. Jawaid, S. Koksal, S. Sharif, J. Mater. Process. Technol. 116 (2001) 2.
[56] E.O. Ezugwu, I.R. Pashby, J. Mater. Process. Technol. 33 (1992) 429.
[57] J. Paulo Davim, "Princípios de Maquinagem", ed. Almelinda, Coimbra, 2005.